RESEARCH FRONT

Full Paper

CSIRO PUBLISHING

Aust. J. Chem. **2009**, *62*, 1108–1118

www.publish.csiro.au/journals/ajc

Ferromagnetic [Mn_3] Single-Molecule Magnets and Their Supramolecular Networks

Ross Inglis,[A] *Giannis S. Papaefstathiou,*[B] *Wolfgang Wernsdorfer,*[C] *and Euan K. Brechin*[A,D]

[A]School of Chemistry, West Mains Road, The University of Edinburgh, Edinburgh, EH9 3JJ, UK.
[B]Laboratory of Inorganic Chemistry, Department of Chemistry, National and Kapodistrian University of Athens, Panepistimiopolis, 157 71 Zografou, Greece.
[C]Institut Néel, CNRS & Université J. Fourier, BP 166, 38042 Grenoble, France.
[D]Corresponding author. Email: ebrechin@staffmail.ed.ac.uk

The complexes [$Mn_3^{III}O$(Et-sao)$_3$(O_2CPh(Cl)$_2$)(MeOH)$_3$(H_2O)] (**1**), [$Mn_3^{III}O$(Et-sao)$_3$(ClO_4)(MeOH)$_3$] (**2**), [$Mn_3^{III}O$(Et-sao)$_3$(O_2Ph(CF_3)$_2$)(EtOH)(H_2O)$_3$] (**3**), and [$Mn_3^{III}O$(Ph-sao)$_3$(O_2C-anthra)(MeOH)$_4$]·Ph-saoH_2 (**4**·Ph-saoH_2) display dominant ferromagnetic exchange interactions leading to molecules with $S = 6$ ground states. The molecules are single molecule magnets (SMM) displaying large effective energy barriers for magnetization reversal. In each case their crystal structures reveal multiple intermolecular H-bonding interactions. Single crystal hysteresis loop measurements demonstrate that these interactions are strong enough to cause a clear field bias, but too weak to transform the spin networks into classical antiferromagnets. These three-dimensional networks of exchange coupled SMMs demonstrate that quantum tunnelling magnetization can be controlled using exchange interactions, suggesting supramolecular chemistry can be exploited to modulate the quantum physics of molecular magnets.

Manuscript received: 23 April 2009.
Manuscript accepted: 16 June 2009.

Introduction

The potential of using single molecule magnets (SMMs) in applications such as information storage and quantum information processing has fuelled the synthesis and characterization of a plethora of beautiful molecules displaying fascinating physical properties.[1] Supramolecular SMMs, in which exchange coupling between the molecules results in quantum behaviour different from that of the individual molecule, are a sub-class of such species that promise a degree of control in the fine tuning of the quantum properties of the original molecular SMMs if the role/importance of the inter-cluster interaction can be understood and manipulated.[2] Using SMMs as the building blocks in the supramolecular assembly of 1D–3D SMM architectures incorporating covalent or non-covalent interactions is thus an important field of study.[3] Until recently SMM characterization has focussed purely on the molecule itself and has often excluded the influence of the molecular environment (i.e. the crystal lattice). Crystal packing effects which include weak interactions (e.g. hydrogen bonding, $\pi\cdots\pi$ interaction etc.) may affect the properties of the individual molecules, although these are most likely to be manifested in the magnetic response at (moderately) low temperatures. We have recently initiated a project to both study crystal packing effects upon SMM behaviour and to attempt to utilize SMMs as building blocks for the construction of supramolecular architectures (i.e. polygons, polyhedra) and extended networks (i.e. coordination polymers).[4] To this end we herein present a small family of exchange-coupled [Mn_3] single-molecule magnets built using derivatized salicyaldoximes (R-saoH_2; Scheme 1; saoH_2 is salicyaldoxime) that self-assemble forming 1D, 2D, and 3D hydrogen-bonded frameworks through multiple O–H$\cdots$O or C–H$\cdots\pi$ interactions.

Results and Discussion

After synthesizing a large family of hexametallic SMMs of general formula [Mn_6O_2(R-sao)$_6$(X)$_2$(L)$_{4-6}$] (R = H, Me, Et, Ph; X = O_2CR′, halide; L = MeOH, EtOH, H_2O, etc.)[5] we turned our attention to making and studying their trimetallic analogues [Mn_3O(R-sao)$_3$(X)(L)$_{3,4}$].[6] These can be made rather easily through several synthetic strategies (see Experimental section for full details and Table 1 for crystallographic information). The reaction of $Mn(ClO_4)_2\cdot 4H_2O$ with the appropriate R-saoH_2 and the appropriate NaO_2CR′ in the appropriate alcohol affords [$Mn_3^{III}O$(Et-sao)$_3$(O_2CPh(Cl)$_2$)(MeOH)$_3$(H_2O)] (**1**), [$Mn_3^{III}O$(Et-sao)$_3$(O_2Ph(CF_3)$_2$)(EtOH)(H_2O)$_3$] (**3**), and [$Mn_3^{III}O$(Ph-sao)$_3$(O_2C-anthra)(MeOH)$_4$]·Ph-saoH_2 (**4**·Ph-saoH_2). If the NaO_2CR is left out, [$Mn_3^{III}O$(Et-sao)$_3$(ClO_4)(MeOH)$_3$] (**2**) is produced. All four complexes have similar structures (Fig. 1, Table 2). Their cores comprise a $\{Mn_3^{III}O\}^{7+}$ oxo-centred triangle whose edges are bridged in a $\eta^1{:}\eta^1{:}\eta^1{:}\mu$-fashion by the doubly deprotonated R-sao^{2-} ligands to form three equatorial Mn–N–O–Mn pathways between the metal ions. The $\eta^1{:}\eta^1{:}\mu$-bridging $^{-}O_2$CR ligands straddle the 'top' of the $\{Mn_3^{III}O$(R-sao$)_3\}^{+}$ moiety in **1**, **3**, and **4**, bonding to two Mn(III) centres. The remaining site on the upper face is occupied by a solvent (alcohol/H_2O) molecule, as are all three axial sites at the base of the molecule, completing the distorted octahedral coordination geometry at each Mn(III) centre; the Jahn–Teller axes being

10.1071/CH09236 0004-9425/09/091108

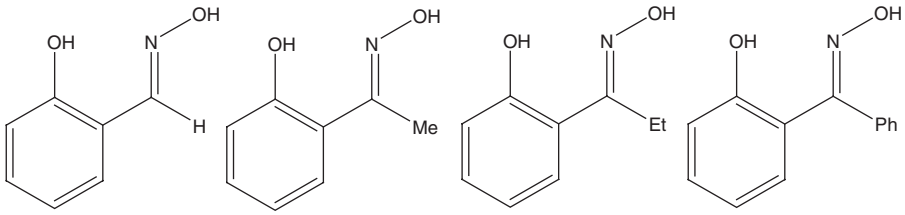

Scheme 1. The R-saoH_2 family of pro-ligands: saoH_2, R = H; Me-saoH_2, R = Me; Et-saoH_2, R = Et; Ph-saoH_2, R = Ph.

Table 1. Crystallographic data for complexes 1–4

	1	**2**	**3**	**4**
Formula	$C_{37}H_{44}Cl_2Mn_3N_3O_{13}$	$C_{30}H_{39}ClMn_3N_3O_{14}$	$C_{40}H_{52}F_6Mn_3N_3O_{16}$	$C_{71}H_{63}Mn_3N_4O_{15}$
M_w	974.46	865.89	1100.63	1377.08
Crystal system	Triclinic	Trigonal	Triclinic	Triclinic
Space group	P-1	R-3	P-1	P-1
a [Å]	12.9349(7)	13.3784(3)	12.2892(4)	13.3430(4)
b [Å]	13.6337(8)	13.3784(3)	13.9947(4)	14.1880(4)
c [Å]	14.5211(8)	34.0617(12)	15.9295(5)	19.3348(5)
α [°]	98.856(4)	90	80.615(2)	94.442(2)
β [°]	96.836(4)	90	70.223(2)	107.421(2)
γ [°]	106.205(3)	120	66.370(2)	109.451(2)
V [Å^3]	2394.1(2)	5279.7(2)	2360.67(13)	3228.60(17)
Z	2	6	2	2
T [K]	150	150	150	150
λ [Å]	0.71073	0.71073	0.71073	0.71073
D_c [g cm^{-3}]	1.352	1.634	1.548	1.416
μ (Mo-K$_\alpha$) [mm^{-1}]	0.948	1.207	0.883	0.649
Meas./indep. (R_{int}) refl.	32694/13347 (0.031)	63184/3607 (0.036)	46784/13042 (0.069)	59334/18844 (0.058)
Obs. refl. [$I > 2\sigma(I)$]	9681	2879	7049	10907
wR_2	0.0429	0.0660	0.1577	0.1119
R_1	0.0395	0.0288	0.0666	0.0470
Goodness of fit on F^2	1.1165	0.8547	0.8888	0.8122
$\Delta\rho_{max,min}$ [e Å^{-3}]	2.06/−0.67	0.62/−0.37	1.85/−1.12	0.86/−0.71

approximately perpendicular to the [Mn_3] plane, tilted at angles ranging between ∼1.7 and 12.5° (Table 2). In **2**, the upper triangular face is capped by a ClO_4^- anion. The effect of the bulky oximes is the generation of relatively 'puckered' or 'twisted' $\{Mn_3^{III}O(\text{R-sao})_3\}^+$ moieties with Mn–N–O–Mn torsion angles in the range ∼33–47°. In each case the central O^{2-} is shifted out of the [Mn_3] plane by distances ranging between ∼0.18 and 0.26 Å (Table 2).

Despite the similarities of the Mn_3 core in all four complexes, the arrangement of the clusters in the crystal lattice is quite different from crystal to crystal due to the differences in the way that the individual molecules interact with each other. Specifically, the molecules in **1** are arranged with their upper faces face-to-face. The water molecule which is attached on the upper face of the Mn_3 triangle is hydrogen bonded to a carboxylate O-atom [∠O2–H22···O24 160.0°, O···O 2.913(2) Å, and H···O 2.130 Å] that belongs to the same cluster and to a phenolate O-atom of a neighbouring cluster [∠O2–H21···O13 $(1-x, -y, -z)$ 174.0°, O···O 2.791(2) Å, and H···O 1.980 Å] creating a hydrogen-bonded dimer (Fig. 2). The dimers assemble with the bases of the Mn_3 triangles face-to-face through two complementary hydrogen bonds that involve a methanolic OH group of one cluster and a phenolate O-atom of a neighbouring cluster [∠O25–H251···O11 $(1-x, -y, 1-z)$ 165.0°, O···O 2.783(2) Å, and H···O 1.980 Å] to create a zig-zag chain that runs parallel to the a axis (Fig. 2). All Mn_3 mean planes within a chain are parallel, with the inter-plane distances being 4.011 Å within a dimer and 3.471 Å between dimers, respectively.

In a manner similar to that of **1**, the clusters of **3** assemble through the coordinated water molecules of the upper face of the Mn_3 triangle and a phenolate O-atom to form a hydrogen-bonded dimer [∠O47–H472···O26 $(1-x, -y, 2-z)$ 156.0°, O···O 2.812(4) Å, and H···O 2.060 Å]. The dimers assemble via the coordinated water and ethanol molecules of the Mn_3 triangle base with the lattice ethanol and water molecules to form a 2D hydrogen-bonded layer that runs parallel to the ab plane (Fig. 3). All Mn_3 mean planes within a layer are again parallel and form an angle of ∼42° with respect to the mean plane of the layer and the ab plane. The intra-plane $Mn_3\cdots Mn_3$ distance within a dimer is 3.929 Å. Alternatively, the hydrogen bonded layer of **3** can be described as being constructed by chains composed of Mn_3 clusters and lattice EtOH and H_2O molecules that run parallel to the a axis (Fig. 3 bottom). The chains are connected to the second dimension via two complementary hydrogen bonds that involve the coordinated water molecules of the upper faces of the Mn_3 triangles and a phenolate O-atom that belongs to a Mn_3 of a neighbouring chain (O47···O26).

The presence of the capping ClO_4^- anion on the upper triangular face of **2** and the absence of solvate molecules forces the Mn_3 clusters to self-assemble through the three MeOH molecules, which are attached on the base of the triangle. Each Mn_3 is hydrogen-bonded to three neighbours through six

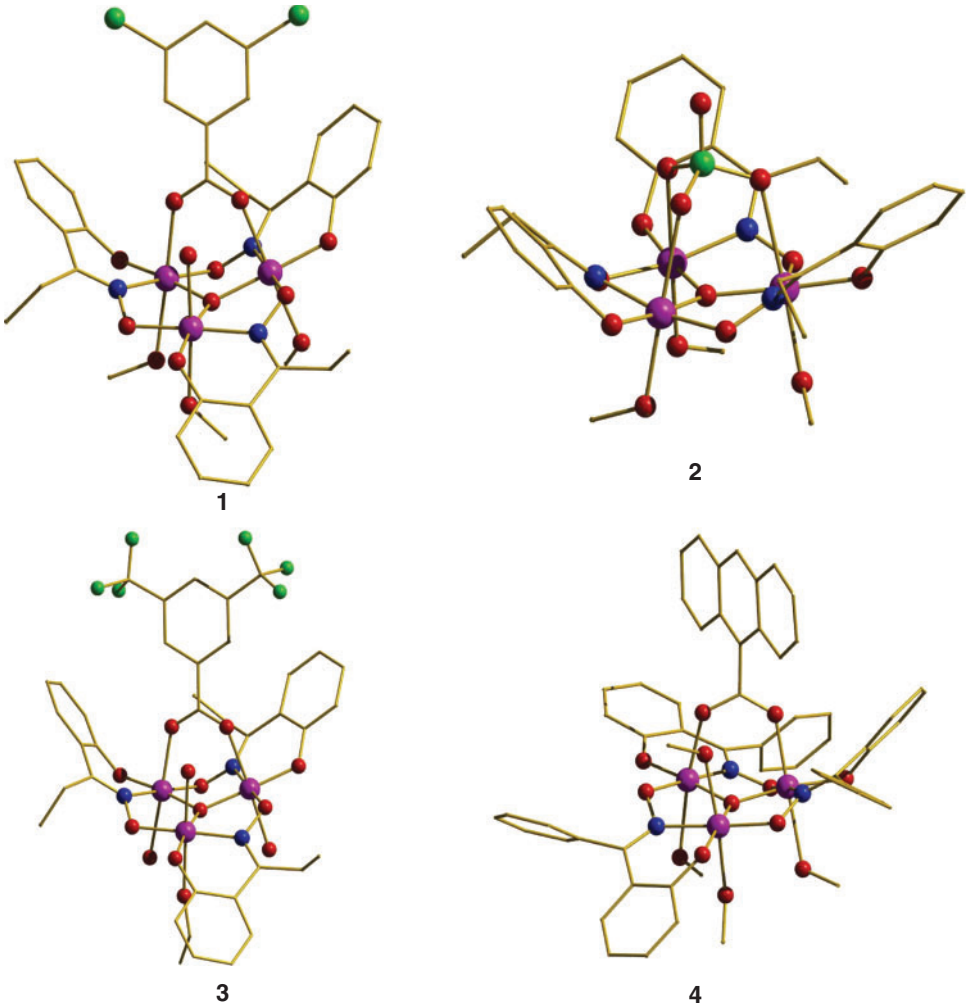

Fig. 1. The molecular structures of **1** (top left), **2** (top right), **3** (bottom left), and **4** (bottom right). Colour code: Mn, purple; O, red; N, blue; halide, green; C, gold.

complementary hydrogen bonds (one unique) that involve the terminal MeOH molecules and the phenolate O atoms of the Et-sao^{2-} ligands [∠O15–H1···O8 $(1-x,\ 1-y,\ 1-z)$ 168°, O···O 2.734(1) Å, and H···O 1.95 Å]. In this arrangement an undulated 2D hydrogen bonded layer forms that conforms to a (6,3) net and lies parallel to the *ab* plane (Fig. 4). The Mn_3 triangles are arranged with their upper faces above and below the plane of the hydrogen-bonded framework with their mean planes parallel to each other and to the mean plane of the framework. The layers stack in an off-set fashion with the Mn_3 triangles of one layer lying above and below the hexagonal cavities of the two neighbouring frameworks.

The Mn_3 clusters in **4** have assembled with a Ph-saoH$_2$ molecule of crystallization (Fig. 5). The MeOH molecule at the upper face of the Mn_3 triangle forms an intra-molecular hydrogen bond with one carboxylate O-atom [∠O18–H18···O24 162°, O···O 2.876(3) Å, and H···O 2.09 Å]. Two of the three MeOH molecules at the base of the triangle are hydrogen-bonded with themselves [∠O17–H17···O15 167°, O···O 2.833(3) Å, and H···O 2.02 Å and ∠O15–H15···O16 171°, O···O 2.695(2) Å, and H···O 1.90 Å] with the third being attached to the Ph-saoH$_2$ molecule [∠O16–H16···N99 163°, O···O 2.751(3) Å, and H···O 1.95 Å]. The salicyl OH group of the Ph-saoH$_2$ molecule forms an intra-molecular hydrogen bond with the oximic O-atom [∠O19–H19···O109 168°, O···O 2.577(3) Å, and H···O 1.69 Å] while the latter attaches to a phenolate O-atom of the triangle [∠O109–H109···O103 163°, O···O 2.643(2) Å, and H···O 1.82 Å]. The Mn_3·Ph-saoH$_2$ units interact with five neighbouring assemblies through 10 (five unique) C–H···π interactions to create a 3D framework with $4^6{\cdot}6^4$-**bnn** topology (Fig. 6).[7]

Direct current (DC) magnetization measurements were carried out on polycrystalline samples of **1**–**4** in a field of 0.1 T and a temperature range of 5–300 K. These are plotted in Fig. 7. Their room temperature $\chi_M T$ values range from ∼9.5 to 11.0 cm^3 mol^{-1} K and are consistent with the expected (spin-only) value for three non-interacting Mn(III) centres (∼9.0 cm^3 mol^{-1} K). All four exhibit dominant ferromagnetic exchange between the Mn(III) ions with the values of $\chi_M T$ increasing with decreasing temperature to maximum values of between ∼13 and 17 cm^3 mol^{-1} K at ∼25 K. This is below the value of ∼21 cm^3 mol^{-1} K expected for an $S = 6$ ground state. Below this temperature a sharp decrease in $\chi_M T$ is observed in each case that can be attributed to a combination of intermolecular interactions (consistent with their crystal structures) and zero-field splitting effects. A simulation of the 'high' temperature (Table 3, Fig. 7) experimental data using the simple 1J model of Eqn (1) and Scheme 2 afforded the parameters

Table 2. Selected bond lengths [Å] and angles [°] for complexes 1–4

Complex	Mn-(μ_3-O) distance [Å]	Mn-(μ_3-O)-Mn angles [°]	Mn_3 plane-μ_3O distance (sd) [Å]	Mn-O_2CR distance/ Mn-O_4Cl [Å]	JT-tilts from Mn_3 mean plane [°]
$[Mn_3O(Etsao)_3(O_2CPh(Cl)_2)(H_2O)(MeOH)_3]$ (**1**)	1.8792(14), 1.8884(13), 1.8738(14)	115.33(7), 120.10(7), 118.71(7)	0.2648(0.0015)	2.2036(15), 2.2082(15)	11.4, 5.8, 7.9
$[Mn_3O(Etsao)_3(MeOH)_3](ClO_4)$ (**2**)	1.8770(2), 1.8791(2), 1.8794(3)	119.150(1), 119.022(7), 119.130(8)	0.1792(0.0017)	2.5496(11)	5.9
$[Mn_3O(Etsao)_3(O_2CPh(CF_3)_2)$ $(EtOH)(H_2O)_3]\cdot EtOH$ (**3**)	1.8803(26), 1.8674(28), 1.8740(26)	115.83(13), 119.96(14), 119.84(14)	0.2274(0.0026)	2.1779(36), 2.3222(28)	6.7, 1.7, 9.0
$[Mn_3O(Phsao)_3(O_2CC_{14}H_{19})$ $(MeOH)_4](PhsaoH_2)$ (**4**)	1.8744(14), 1.8710(17), 1.8696(16)	115.80(8), 121.54(8), 119.98(8)	0.1778(0.0015)	2.1665(22), 2.2059(19)	5.3, 12.5, 3.3

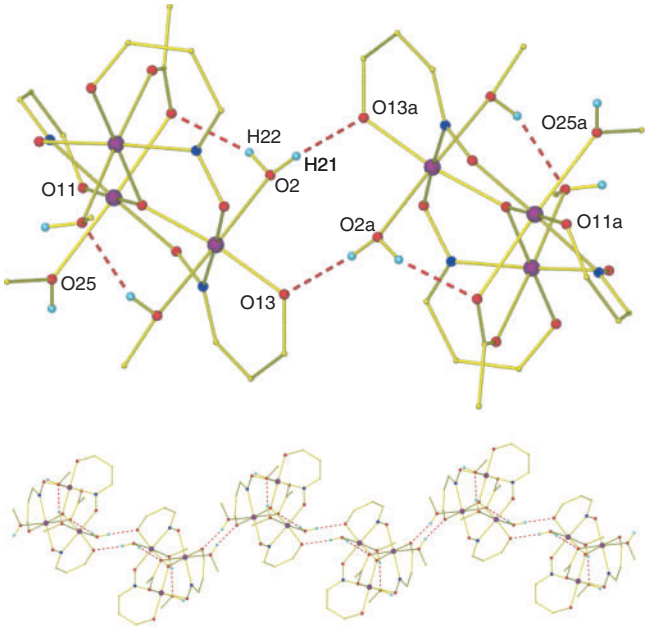

Fig. 2. The hydrogen bonded dimer (top) and the chain (bottom) of **1**. Most hydrogen and carbon atoms have been omitted for clarity. Colour code: Mn, purple; O, red; N, blue; C, gold; H, cyan. Symmetry code: a: $1-x, -y, -z$.

$S = 6$, $g = 2.02$, and $J = +1.84\,cm^{-1}$ for **1**; $S = 6$, $g = 2.02$, and $J = +2.80\,cm^{-1}$ for **2**; and $S = 6$, $g = 1.98$, and $J = +1.52\,cm^{-1}$ for **3**. The same model proved unsuccessful for **4**, which required the 2J model of Eqn (2) and Scheme 2, giving $S = 6$, $g = 1.98$, $J_1 = +0.85\,cm^{-1}$, and $J_2 = +1.44\,cm^{-1}$ (Table 3). It is clear from Fig. 7 that intermolecular interactions are playing a very important role in the observed behaviour for all four complexes, with only the data for complex **3** being satisfactorily simulated down to even moderately low temperatures. Thus we add a note of caution to the absolute validity/accuracy of the simulation parameters, although they are well within the range observed for *all* previously reported (and analogous) salicyaldoxime-bridged [Mn(III)$_3$]and [Mn(III)$_6$] clusters (Scheme 2).[5,6]

$$\hat{H} = -2J[(\hat{S}_1 \cdot \hat{S}_2) + (\hat{S}_2 \cdot \hat{S}_3) + (\hat{S}_1 \cdot \hat{S}_3)] \quad (1)$$

$$\hat{H} = -2J_1[(\hat{S}_1 \cdot \hat{S}_2) + (\hat{S}_2 \cdot \hat{S}_3)] - 2J_2[(\hat{S}_1 \cdot \hat{S}_3)] \quad (2)$$

In order to confirm the spin ground state and *attempt* to determine $|D|$, magnetization data were collected in the ranges 0.5–7.0 T and 2–7 K for all four complexes. Representative reduced magnetisation ($M/N\beta$) versus H/T data for complexes **1** and **3** are given in Fig. 8. In each case the data saturate below $M/N\beta = 12$ indicative of an $S = 6$ state with significant $|D|$. Fitting of the high field, low temperature experimental data (Table 3) with the axial zero field splitting (ZFS) plus Zeeman Hamiltonian of Eqn (3), which assumes only the ground state is populated, afforded $S = 6$, $g = 1.98$, and $D = -0.59\,cm^{-1}$ for **1**; $S = 6$, $g = 1.98$, and $D = -0.77\,cm^{-1}$ for **2**; $S = 6$, $g = 1.98$, and $D = -0.82\,cm^{-1}$ for **3**; and $S = 6$, $g = 1.98$, and $D = -0.51\,cm^{-1}$ for **4**. Although the fits of Fig. 8 look rather good, an abnormality is immediately present: despite the four complexes being rather similar, the calculated D values span a wide range from $\sim 0.5\,cm^{-1}$ to $0.8\,cm^{-1}$, and therefore must be treated with caution. Although one would expect some variation due to the varying Jahn–Teller tilts, it is clear that the strong intermolecular interactions, disorder (in **3**)

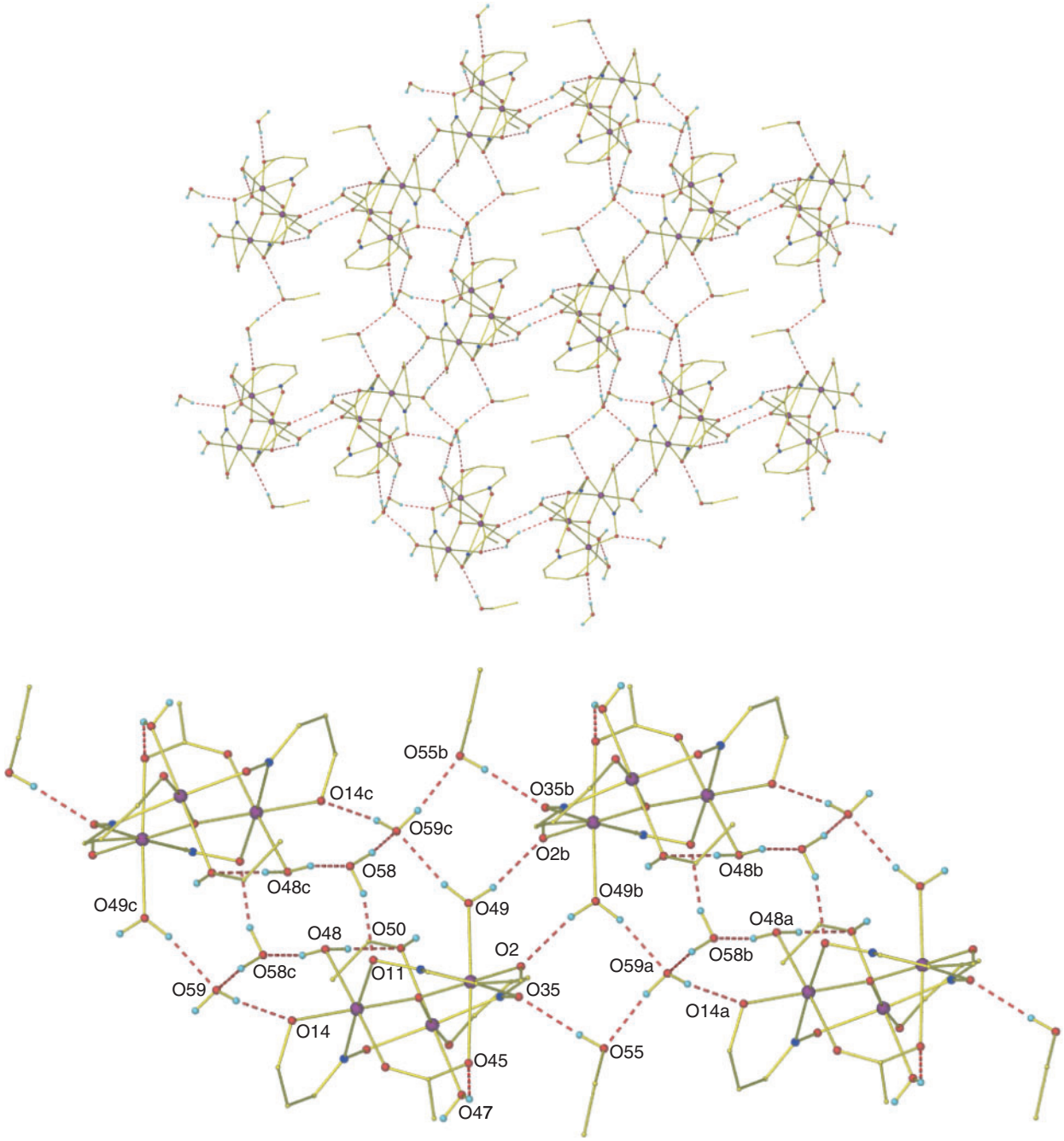

Fig. 3. The hydrogen bonded layer (top) and the chain (bottom) in **3**. Colour code: Mn, purple; O, red; N, blue; C, gold; H, cyan. Most hydrogen and carbon atoms have been omitted for clarity. Symmetry codes: a: $x-1, y, z$; b: $-x, 1-y, 2-z$; c: $1-x, 1-y, 2-z$.

which causes a distribution in molecular environments, the presence of weak exchange and thus the likely population of excited states in the temperature range studied, and the simplistic model employed, do not allow for an accurate determination of D. Indeed, magnetization and high frequency electron paramagnetic resonance studies of analogous molecules in which there are no intermolecular interactions suggest $|D|$ values $\geq 0.8\ \mathrm{cm}^{-1}$, which would be consistent only with **3**.[8] Further proof for this assumption emerges in the analysis of the alternating current (AC) data and single crystal hysteresis loop measurements discussed below.

$$\hat{H} = D(\hat{S}_z^2 - S(S+1)/3) + \mu_B g H \hat{S} \qquad (3)$$

AC susceptibility studies were carried out on crystalline samples of **1**–**4** in the 1.8–10.0 K range in a 3.5 G field oscillating at frequencies between 50 and 1000 Hz. Frequency-dependent out-of-phase (χ''_{M}) signals suggestive of SMM behaviour were observed for all four complexes with peaks at ~4.5–5.0 K at a frequency of 1000 Hz for **1**–**3**, with only the tails of peaks visible for **4**. Those for complex **3** are shown in Fig. 9. In each case the AC data were used to construct Arrhenius plots (Fig. 9) from which fitting of the Arrhenius equation gave $U_{eff} \approx 43.7$ K, $\tau_0 = 1.27 \times 10^{-9}$ s for **1**; $U_{eff} \approx 57.0$ K, $\tau_0 = 1.98 \times 10^{-9}$ s for **2**; and $U_{eff} \approx 42.5$ K, $\tau_0 = 7.40 \times 10^{-9}$ s for **3**. These are among the largest effective barriers observed for any low nuclearity SMMs, but they are also *larger* than the theoretical

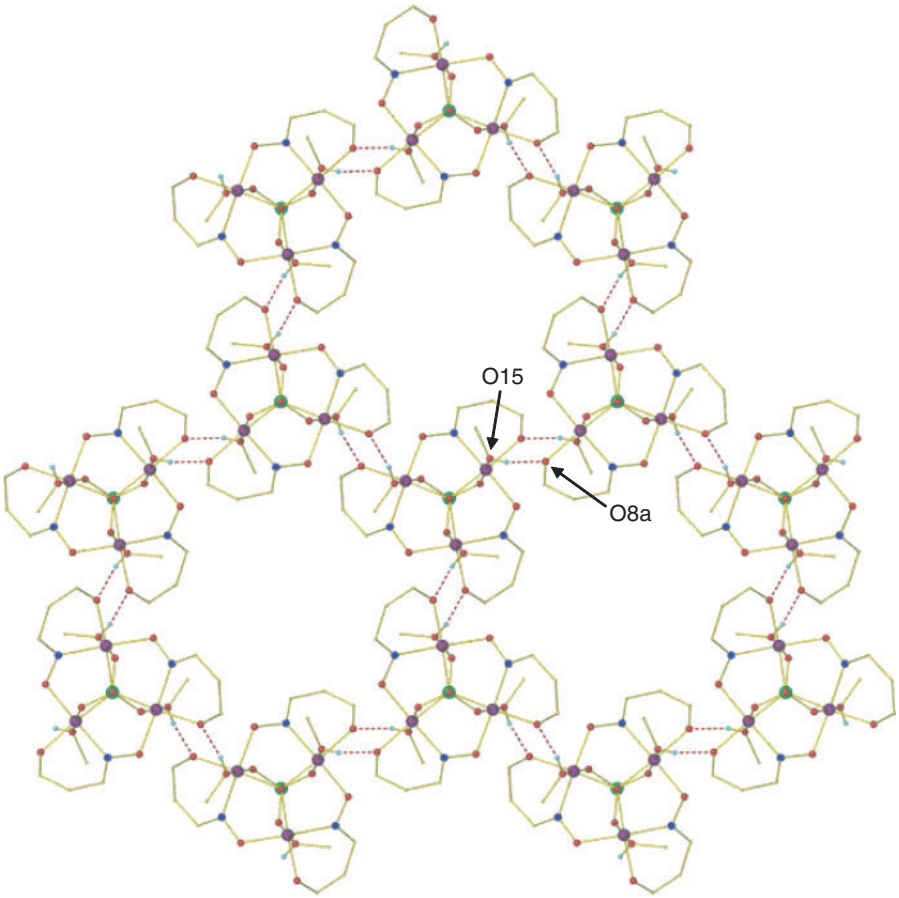

Fig. 4. The hydrogen bonded (6,3) layer in **2**. Colour code: Mn, purple; O, red; N, blue; Cl, green; C, gold; H, cyan. Most hydrogen and carbon atoms have been omitted for clarity. Symmetry code: a: $1-x$, $1-y$, $1-z$.

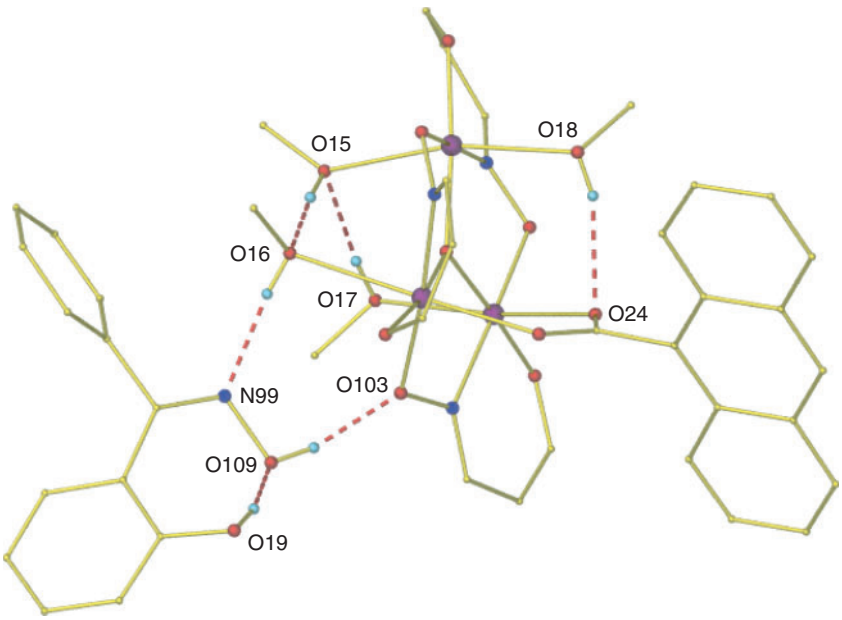

Fig. 5. The hydrogen bonded Mn_3·Ph-saoH_2 assembly in **4**. Most hydrogen and carbon atoms have been omitted for clarity. Colour code: Mn, purple; O, red; N, blue; C, gold; H, cyan.

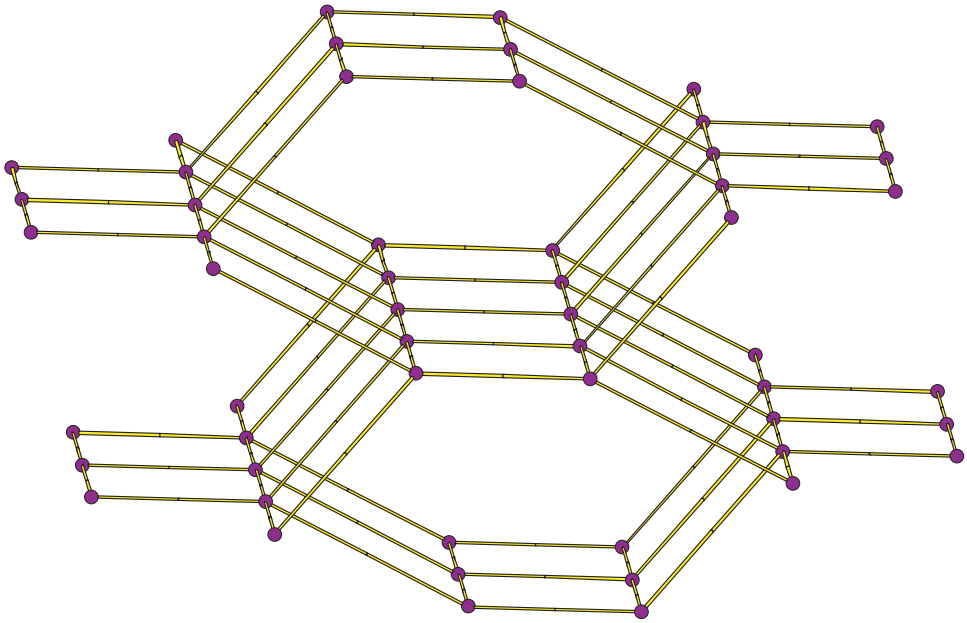

Fig. 6. The $4^6{\cdot}6^4$-**bnn** hydrogen bonded network found in **4**. Purple spheres represent the $Mn_3{\cdot}$Ph-saoH_2 assemblies while the gold lines represent the C–H$\cdots\pi$ interactions.

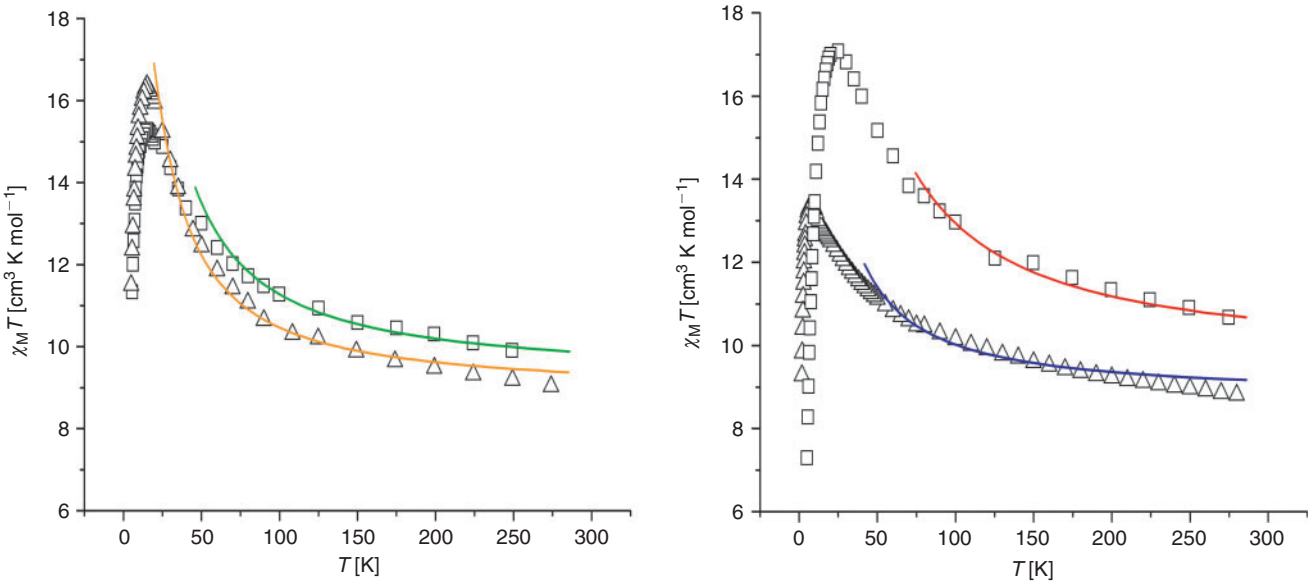

Fig. 7. Plots of $\chi_M T$ versus T for **1**–**4**. The solid lines represent simulations of the experimental data. See text for full details.

upper limit [$U = S^2|D|$] calculated using the D values obtained from the powder DC magnetization measurements (~30 K (**1**); ~40 K (**2**); ~42 K (**3**)). Indeed, again only complex **3** has an experimental value close to its theoretical value. This is to be expected for exchange-coupled SMMs because the spin reversal is hindered by the relatively weak intermolecular coupling. For stronger intermolecular exchange coupling one would move away from the biased-SMM regime into a 3D system where the collective modes (domain wall propagation etc.) would reduce the effective barriers. It also points to a possible underestimation in the ZFS parameters obtained from the powder DC measurements, which is confirmed in the single crystal low temperature magnetization studies.

Hysteresis loop and relaxation measurements were carried out on single crystals of **1**–**4** using a micro-SQUID assembly, with the field applied along the easy axis of magnetization.[9] In each case temperature and sweep rate dependent hysteresis loops were observed, confirming SMM behaviour for all four complexes. Representative examples are shown for complexes **2** and **3** in Fig. 10. In each case the loops display step-like features separated by plateaus. After saturating the magnetization, the first resonance is seen in negative fields. This is indicative of the presence of small and antiferromagnetic intermolecular interactions and was first observed in the complex $[Mn_4O_3Cl_4(O_2CEt)_3(py)_3]$, which crystallizes as a supramolecular H-bonded dimer of cubanes ($[Mn_4]_2$).[3] The hysteresis

Table 3. Magneto-structural pararmeters for complexes 1–4

Complex	Crystal system	Space group	α [°] Mn1–2/Mn2–3/Mn1–3	J [cm^{-1}][A] $J_1/J_2/J_3$	S^B	1 $st_{exc.\ st.}$ [cm^{-1}][B]	g^C	D [cm^{-1}][D]	τ_0 [s][E]	U_{eff} [K][F]	θ [K][A]
1	Triclinic	P-1	44.60, 38.17, 39.07	+1.84	6	5(22.08)	2.02	−0.59	1.27×10^{-9}	43.69	27.82
2	Trigonal	R-3	42.12	+2.80	6	5(33.6)	2.06	−0.77	1.98×10^{-9}	57.02	30.77
3	Triclinic	P-1	46.66, 38.56, 40.35	+1.52	6	5(18.24)	1.98	−0.82	7.40×10^{-9}	42.53	16.98
4	Triclinic	P-1	32.98, 34.41, 41.44	+0.85, +1.44	6	5(13.8)	1.98	−0.51			20.44

[A]Calculated from DC susceptibility studies.
[B]Calculated from both DC susceptibility and magnetization measurements. The latter were collected in the field and temperature ranges 0–7 T and 2–7 K. In each case the data were fit by a matrix-diagonalization method to a model that assumes only the ground state is populated, includes axial zero-field splitting ($D\hat{S}_z^2$), and carries out a full powder average. The corresponding Hamiltonian is $H = D(\hat{S}_z^2 - S(S+1)/3) + \mu_B g H \hat{S}$, where D is the axial anisotropy, μ_B is the Bohr magneton, $\hat{S}_z$ is the easy-axis spin operator, and H is the applied field.
[C]Calculated from DC susceptibility measurements.
[D]Calculated from magnetisation measurements.
[E,F]Calculated from DC susceptibility data and/or single-crystal relaxation measurements performed on a micro-SQUID.

Scheme 2. The interaction scheme employed to simulate the $\chi_M T$ versus T data for **2** (left) and **1**, **3**, and **4** (right). For **1** and **3** $J_1 = J_2$.

loops show that the collective spins of each [Mn_3] are coupled antiferromagentically to its neighbouring molecules, acting as a bias that shifts the quantum tunnelling resonances with respect to the isolated SMM. The majority of the small steps observed in all the loops are due to molecules having one (or several) 'reversed' (spin up–spin down) neighbouring molecules – although some may be attributed to multi-body quantum effects.[10] The complexity of the 3D H-bonding networks seen in the crystal structures of **1**–**4** makes it essentially impossible (or at least extremely difficult) to determine all of the active exchange paths and to identify all of the steps. However, for **3** for example, the field separation between the first and second biggest steps for fast field sweep rates can be estimated as $D \approx 1.1\ cm^{-1}$ leading to a barrier of $DS^2 = 58$ K. This is somewhat larger than the effective barrier from the AC data and consistent with earlier comments regarding the validity of the D values obtained from the fit of the magnetization versus field data, and with previous reports of analogous 'uncoupled' [Mn_3^{III}] triangles; i.e. the magnitude of D for all four complexes appears to be somewhat underestimated. New clusters with these intermolecular interactions removed will be required to get an accurate representation of the spin Hamiltonian parameters and of the relaxation dynamics.

Conclusions

[Mn(III)$_3$] triangles can be synthesized using a combination of bulky derivatized salicylaldoximes (R-saoH$_2$) and bulky carboxylates in alcohol. Steric considerations result in 'non-planar' or 'puckered' trimetallic units with the terminally bonded water or alcohols H-bonding to nearest neighbours creating supramolecular networks with various dimensionalities. Magnetic studies reveal dominant ferromagnetic exchange between the metal centres resulting in the observation of single-molecule magnetism behaviour. The multi-dimensional networks formed in the crystal show that exchange coupled SMMs do not suppress quantum tunnelling of the magnetization (QTM). The intermolecular interactions are strong enough to cause a clear field bias, but too weak to transform the spin network into a classical antiferromagnet. Such networks of exchange coupled SMMs demonstrate that QTM can potentially be controlled using exchange interactions and this opens up new perspectives for the use of supramolecular chemistry in the modulation of the quantum physics of molecular nanomagnets. By the same token these intermolecular interactions make derivation of the intra-triangle exchange parameters extremely difficult and accurate representation can only be obtained through the synthesis of 'magnetically isolated' family members; i.e. the terminal alcohol molecules must be replaced with non-H-bonding substituents

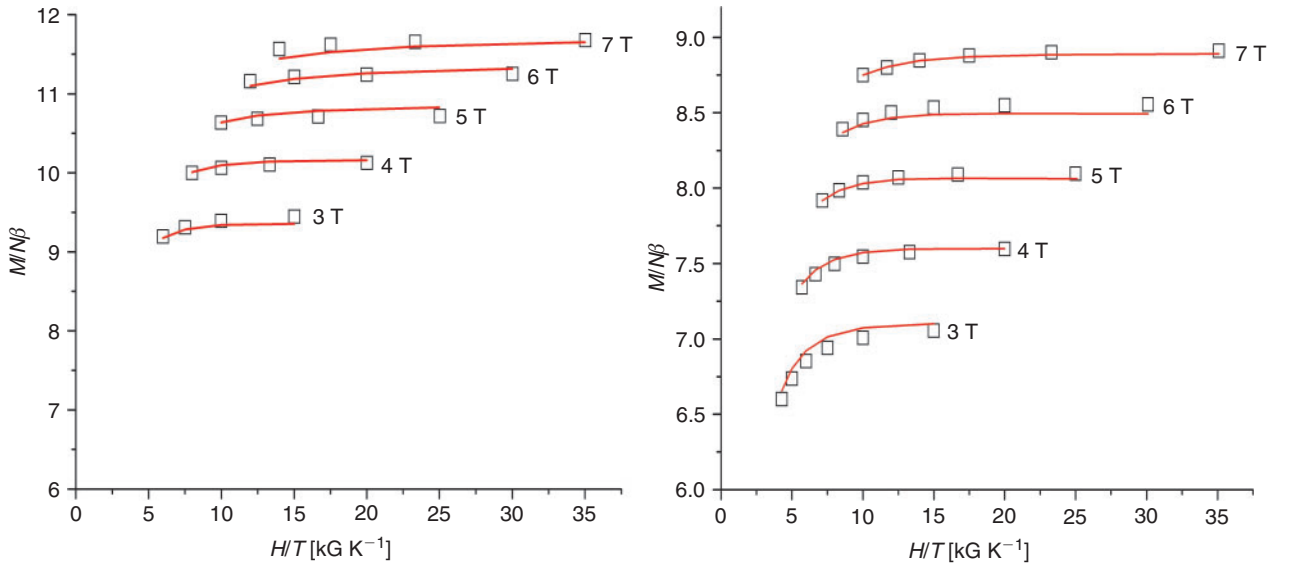

Fig. 8. Plot of reduced magnetization ($M/N\beta$) versus H/T for complexes **1** (left) and **3** (right). The solid lines represent fits to the experimental data. See text and Table 3 for best fit parameters and comments.

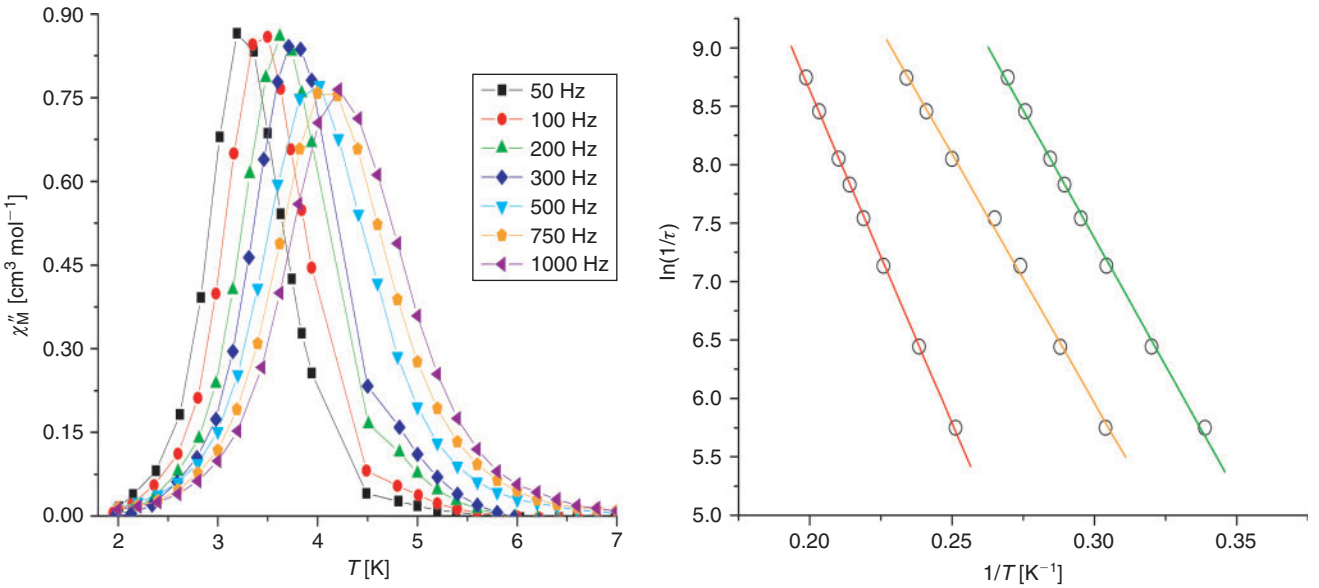

Fig. 9. Out-of-phase (χ''_M) AC susceptibility versus temperature for complex **3** (left) and the Arrhenius plots [$\ln(1/\tau)$ versus $1/T$] for **1**–**3** (right). See text and Table 3 for best fit parameters and comments.

and the disorder must be removed. Simple SMMs in which the influence of intermolecular interactions and excited states are negligible at low temperatures potentially represent an exciting discovery because it will give us access to simple molecules containing only three metal ions that display SMM behaviour and tunnel effects, and thus potential model systems with which to go beyond the giant spin approximation to yield much fruitful physical information.

Experimental

All manipulations were performed under aerobic conditions, using materials as received. CAUTION! Although no problems were encountered in this work, care should be taken when using the potentially explosive perchlorate anion.

Variable temperature, solid-state DC and AC magnetic susceptibility data down to 1.8 K were collected on a Quantum Design MPMS-XL SQUID magnetometer equipped with a 7 T DC magnet. Diamagnetic corrections were applied to the observed paramagnetic susceptibilities using Pascal's constants. Magnetic studies below 1.8 K were carried out on single crystals using a micro-SQUID apparatus operating down to 40 mK.

Diffraction data were collected at 150 K on a Bruker Smart Apex CCDC diffractometer, equipped with an Oxford Cryosystems LT device, using Mo radiation. See Table 1 for full details. CCDC-667576 (**1**), CCDC-694669 (**2**), CCDC-667575 (**3**), CCDC-667577 (**4**) contain the supplementary crystallographic data for this paper. These data can be obtained free of charge from The Cambridge Crystallographic Data Centre via www.ccdc.cam.ac.uk/data_request/cif.

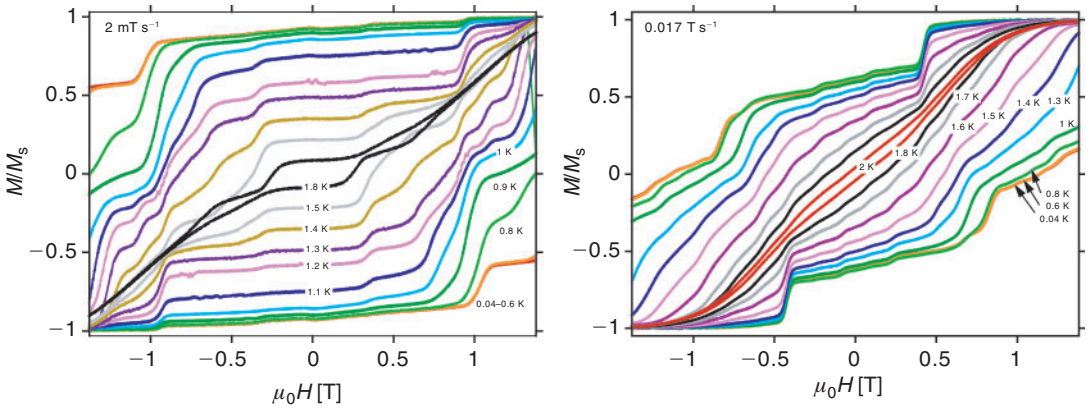

Fig. 10. Magnetization versus field hysteresis loops, measured along the easy-axis of magnetisation, for a single crystal of **2** (left) and **3** (right) at the indicated temperatures and field sweep rates. *M* is normalized to its saturation value.

*$[Mn^{III}_3O(Et\text{-}sao)_3(\mu_2\text{-}O_2CPhCl_2)(MeOH)_3(H_2O)]$ (**1**)*

$Mn^{II}(ClO_4)_2{\cdot}6H_2O$ (0.25 g, 0.98 mmol), Et-saoH$_2$ (0.17 g, 1 mmol), $Cl_2PhCOOH$ (0.39 g, 2 mmol), and NaOMe (0.16 g, 3 mmol) were dissolved in 25 mL of MeOH. After stirring for 1 h, the resulting dark green solution was filtered and left for slow evaporation. X-ray quality crystals of **12** were obtained from the mother liquor over the course of 1 week. Elemental analysis [%]: calc. for $C_{37}H_{44}Cl_2N_3O_{13}Mn_3$: C 45.60, H 4.55, N 4.31; found: C 45.58, H 3.38, N 4.65.

*$[Mn^{III}_3O(Et\text{-}sao)_3(ClO_4)(MeOH)_3]$ (**2**)*

$Mn^{II}(ClO_4)_2{\cdot}6H_2O$ (0.25 g, 0.98 mmol), Et-saoH$_2$ (0.17 g, 1 mmol), and a 1.0 M aqueous solution of $NEt_4(OH)$ (2 mL) were dissolved in 25 mL of MeOH. After stirring for 1 h, the resulting dark green solution was filtered and left for slow evaporation. X-ray quality crystals of **12** were obtained from the mother liquor over the course of 1 week. Elemental analysis [%]: calc. for $C_{30}H_{39}N_3O_{14}ClMn_3$: C 41.61, H 4.54, N 4.81; found: C 41.32, H 4.76, N 5.03.

*$[Mn_3O(Et\text{-}sao)_3(\mu_2\text{-}O_2Ph(CF_3)_2)(EtOH)(H_2O)_3]{\cdot}EtOH{\cdot}3H_2O$ (**3**·EtOH·3H$_2$O)*

$Mn^{II}(ClO_4)_2{\cdot}6H_2O$ (0.25 g, 0.98 mmol), Et-saoH$_2$ (0.167 g, 0.98 mmol), and $NaO_2Ph(CF_3)_2$ (0.137 g, 0.49 mmol) were dissolved in 25 cm^3 EtOH. 20 drops of an 1.0 M aqueous solution of $NEt_4(OH)$ was added slowly to afford a black solution which was left to stir for 1 h. After filtration the solution was left to evaporate slowly. X-ray quality crystals of **15** were afforded in 30% yield after 3 days. Microanalysis: calc. for $C_{38}H_{44}N_3O_{14}F_6Mn_3$ (**15**·H_2O): C 43.65, H 4.24, N 3.85; found: C 43.46, H 4.32, N 3.85.

*$[Mn^{III}_3O(Ph\text{-}sao)_3(\mu_2\text{-}O_2C_{15}H_9)(MeOH)_4]{\cdot}(Ph\text{-}saoH_2)$ (**4**·Ph-saoH$_2$)*

$Mn^{II}(ClO_4)_2{\cdot}6H_2O$ (0.25 g, 0.98 mmol), Ph-saoH$_2$ (0.21 g, 0.98 mmol), $C_{14}H_9COOH$ (0.22 g, 0.98 mmol), and NEt_4OH (0.15 g, 0.98 mmol) were dissolved in 25 mL of MeOH. After stirring for 1 h, the resulting dark green solution was filtered and X-ray quality crystals of **6** were obtained upon slow evaporation after 4 days. Elemental analysis [%]: calc. for $C_{71}H_{63}N_4O_{15}Mn_3$: C 61.93, H 4.61, N 4.07; found: C 61.92, H 4.53, N 4.13.

References

[1] (a) D. Gatteschi, R. Sessoli, *Angew. Chem. Int. Ed.* **2003**, *42*, 268. doi:10.1002/ANIE.200390099
(b) D. Gatteschi, R. Sessoli, J. Villain, *Molecular Nanomagnets*. **2006** (Oxford University Press), and references therein.
(c) G. Aromí, E. K. Brechin, *Struct. Bonding* **2006**, *122*, 1. doi:10.1007/430_022
(d) R. Bircher, G. Chaboussant, C. Dobe, H. U. Güdel, S. T. Ochsenbein, A. Sieber, O. Waldmann, *Adv. Funct. Mater.* **2006**, *16*, 209. doi:10.1002/ADFM.200500244

[2] (a) H. Miyasaka, M. Yamashita, *Dalton Trans.* **2007**, 399. doi:10.1039/B614582E
(b) O. Roubeau, R. Clérac, *Eur. J. Inorg. Chem.* **2008**, 4325. doi:10.1002/EJIC.200800603
(c) J. Yoo, W. Wernsdorfer, E.-C. Yang, M. Nakano, A. L. Rheingold, D. N. Hendrickson, *Inorg. Chem.* **2005**, *44*, 3377. doi:10.1021/IC048212A
(d) L. M. Wittick, K. S. Murray, B. Moubaraki, S. R. Batten, L. Spiccia, K. J. Berry, *Dalton Trans.* **2004**, 1003. doi:10.1039/B312672B

[3] (a) W. Wernsdorfer, N. Aliaga-Alcalde, D. N. Hendrickson, G. Christou, *Nature* **2002**, *416*, 406. doi:10.1038/416406A
(b) S. Hill, R. S. Edwards, N. Aliaga-Alcalde, G. Christou, *Science* **2003**, *302*, 1015. doi:10.1126/SCIENCE.1090082

[4] (a) L. F. Jones, A. Collins, S. Parsons, M. Evangelisti, E. K. Brechin, *Chem. Commun.* **2009**, 2023. doi:10.1039/B900743A
(b) C. C. Stoumpos, R. Inglis, G. Karotsis, L. F. Jones, A. Collins, S. Parsons, C. J. Milios, G. S. Papaefstathiou, E. K. Brechin, *Cryst. Growth Des.* **2009**, *9*, 24. doi:10.1021/CG800947Z
(c) G. Karotsis, C. Stoumpos, A. Collins, F. White, S. Parsons, A. M. Z. Slawin, G. S. Papaefstathiou, E. K. Brechin, *Dalton Trans.* **2009**, 3388. doi:10.1039/B902002K
(d) G. Karotsis, L. F. Jones, G. S. Papaefstathiou, A. Collins, S. Parsons, T. D. Nguyen, M. Evangelisti, E. K. Brechin, *Dalton Trans.* **2008**, 4917. doi:10.1039/B804897E

[5] (a) See for example: R. Inglis, L. F. Jones, C. J. Milios, S. Datta, A. Collins, S. Parsons, W. Wernsdorfer, S. Hill, S. P. Perlepes, S. Piligkos, E. K. Brechin, *Dalton Trans.* **2009**, 3403. doi:10.1039/B822235E
(b) C. J. Milios, R. Inglis, A. Vinslava, R. Bagai, W. Wernsdorfer, S. Parsons, S. P. Perlepes, G. Christou, E. K. Brechin, *J. Am. Chem. Soc.* **2007**, *129*, 12505. doi:10.1021/JA0736616
(c) C. J. Milios, A. Vinslava, W. Wernsdorfer, A. Prescimone, P. A. Wood, S. Parsons, S. P. Perlepes, G. Christou, E. K. Brechin, *J. Am. Chem. Soc.* **2007**, *129*, 6547. doi:10.1021/JA070411G
(d) C. J. Milios, A. Vinslava, S. Moggach, S. Parsons, W. Wernsdorfer, G. Christou, S. P. Perlepes, E. K. Brechin, *J. Am. Chem. Soc.* **2007**, *129*, 2754. doi:10.1021/JA068961M
(e) C. J. Milios, A. Vinslava, P. A. Wood, S. Parsons, W. Wernsdorfer,

G. Christou, S. P. Perlepes, E. K. Brechin, *J. Am. Chem. Soc.* **2007**, *129*, 8. doi:10.1021/JA0666755

[6] (a) C. J. Milios, R. Inglis, L. F. Jones, A. Prescimone, S. Parsons, W. Wernsdorfer, E. K. Brechin, *Dalton Trans.* **2009**, 2812. doi:10.1039/B820362H
(b) R. Inglis, L. F. Jones, G. Karotsis, A. Collins, S. Parsons, S. P. Perlepes, W. Wernsdorfer, E. K. Brechin, *Chem. Commun.* **2008**, 5924. doi:10.1039/B811796A
(c) R. Inglis, L. F. Jones, K. Mason, S. P. Perlepes, W. Wernsdorfer, E. K. Brechin, *Chem. Eur. J.* **2008**, *14*, 9117. doi:10.1002/CHEM.200801266
(d) J. Cano, T. Cauchy, E. Ruiz, C. J. Milios, T. T. Stamatatos, S. P. Perlepes, G. Christou, E. K. Brechin, *Dalton Trans.* **2008**, 234. doi:10.1039/B710055H
(e) C. J. Milios, P. A. Wood, S. Parsons, D. Foguet-Albiol, C. Lampropoulos, G. Christou, S. P. Perlepes, E. K. Brechin, *Inorg. Chim. Acta* **2007**, *360*, 3932. doi:10.1016/J.ICA.2007.06.031
(f) C. J. Millos, A. G. Whittaker, E. K. Brechin, *Polyhedron* **2007**, *26*, 1927. doi:10.1016/J.POLY.2006.09.072

[7] (a) M. O'Keeffe, M. A. Peskov, S. J. Ramsden, O. M. Yaghi, *Acc. Chem. Res.* **2008**, *41*, 1782. doi:10.1021/AR800124U
(b) http://www.topos.ssu.samara.ru; V. A. Blatov, *IUCr CompComm Newsletter* **2006** *7*, 4.

[8] (a) R. Inglis, S. Hill, W. Wernsdorfer, E. K. Brechin, *Inorg. Chem.* **2009**, *48*, 3480.
(b) P. L. Feng, C. Koo, J. J. Henderson, M. Nakano, S. Hill, E. del Barco, D. N. Hendrickson, *Inorg. Chem.* **2008**, *47*, 8610. doi:10.1021/IC801208Z
(c) P. L. Feng, C. Koo, J. J. Henderson, P. Manning, M. Nakano, E. del Barco, S. Hill, D. N. Hendrickson, *Inorg. Chem.* **2009**, *48*, 3480. doi:10.1021/IC802336K

[9] (a) W. Wernsdorfer, *Adv. Chem. Phys.* **2001**, *118*, 99. doi:10.1002/9780470141786.CH3
(b) W. Wernsdorfer, *Supercond. Sci. Technol.* **2009**, *22*, 064013. doi:10.1088/0953-2048/22/6/064013

[10] (a) R. Tiron, W. Wernsdorfer, N. Aliaga-Alcalde, G. Christou, *Phys. Rev. B* **2003**, *68*, 140407. doi:10.1103/PHYSREVB.68.140407
(b) W. Wernsdorfer, S. Bhaduri, R. Tiron, D. N. Hendrickson, G. Christou, *Phys. Rev. Lett.* **2002**, *89*, 19720. doi:10.1103/PHYSREVLETT.89.197201
(c) W. Wernsdorfer, S. Bhaduri, A. Vinslava, G. Christou, *Phys. Rev. B,* **2005**, *72*, 214429.